Progress In Electromagnetics Research C, Vol. 124, 227–242, 2022

Design Improvements in Double-Stator Axial Flux Switched Reluctance Motor for Smoother Torque Profile

Kalpana Chaudhary[1, *], Manoj Pokhriyal[1], and Ayushi Chaudhary[2]

Abstract—High torque and power generation capability of double-stator axial flux switched reluctance motor (DSAFSRM) makes it superior to conventional and segmented rotor switched reluctance motors. Despite its significant feature, the ripple in developed torque still limits the usefulness of DSAFSRM for widespread industrial application. This paper proposes an 8/6/8 pole DSAFSRM with modification in rotor pole shape to reduce torque ripples in respective model. The respective phase windings of the upper and lower stators are excited externally by preparing the circuit in Maxwell software. Each rotor tooth is constructed with two types of slots with different levels of air gap to change the inductance profile. Firstly, the design of a conventional DSAFSRM has been presented; thereafter, some geometric modifications in the rotor tooth have been suggested and investigated to obtain a lower torque ripple at 1200 rpm in the proposed DSAFSRM. The efficacy of the proposed motor is investigated through finite element method (FEM) based analysis and also by comparative analysis with other types of switched reluctance motors. It can be inferred from the simulation results that the torque ripple is significantly reduced by 55.62% in the proposed DSAFSRM compared to the conventional DSAFSRM. However, the efficiency of the proposed DSAFSRM (73.87%) is slightly less than the conventional DSAFSRM (74.65%).

1. INTRODUCTION

The key features of switched reluctance motor (SRM) like simple construction with no rotor winding, high torque/weight ratio, low cost converter requirement, and unipolar switching make it a strong competitor for Industrial drive [1–4]. Low cost converter with only one controllable switch per phase can conveniently meet the unipolar excitation requirement of SRMs [5, 6]. High torque to weight ratio and simple construction make it a potential candidate for various specialized applications like E-mobility, agricultural purpose, aerospace applications, flywheel energy system, and household appliances [7–12]. However, research is underway to overcome some drawbacks such as low efficiency, low torque/power density, high torque ripple, and high vibrations. Several researches have been reported in the literature to improve these parameters. Improvement in the developed torque in segmental rotor SRM (SSRM) is observed in [13]. High silicon steel is most suitable for improving the efficiency of SRM [14]. Two types of torque ripple mitigation techniques have been prominently reported in the literature. Structural design modification, also referred as passive method, can bring the torque ripple reduction in machines [15]. The turn on and turn off angle optimization of power converter can also mitigate the ripples in average torque [16]. The shaping of phase currents through controlled switching of the converter, also called as active method, is employed to reduce the torque ripple [17, 18]. Constant instantaneous torque can be achieved by regulating the speed of stator flux linkage [19]. A simplified control method for direct and simultaneous control of torque in single-winding bearing less SRM is presented in [20]. A fixed switching

Received 11 July 2022, Accepted 9 September 2022, Scheduled 28 September 2022

* Corresponding author: Kalpana Chaudhary (kchaudhary.eee@iitbhu.ac.in).

[1] Department of Electrical Engineering, Indian Institute of Technology (B.H.U.), Varanasi, India. [2] Department of Electrical Engineering, Indian Institute of Technology Kanpur, India.

frequency deadbeat control algorithm to accomplish active method reduced the torque ripple in [33]. DSAFSRMs having two stators and a toothed rotor further improve torque/power density. However, it suffers from the drawback of poor efficiency and high torque ripple. A second-order sliding mode speed controller is presented to reduce the torque ripple of bearing less DSSRM in [21]. ANSYS software based electromagnetic analysis of SRM is explored in [22]. This paper presents the design procedure of 8\6\8 DSAFSRM with a multilevel air gap and pole shoe to mitigate the torque ripple. Slot fill factor (S.F.F) is taken as 0.43 [30–32] and average current density taken as 12 A/sq mm. As our both stators at the outer stator are exposed to environment this could be the permissible limit for thermal consideration. The efficacy of the proposed geometry is tested by doing software based comparative electromagnetic analysis with some reported DSAFSRMs.

1.1. Conventional DSAFSRM Analysis

The constructional layout of a 4-phase 8\6\8 pole single-tooth winding DSAFSRM is shown in Figs. 1(a) and 1(b).

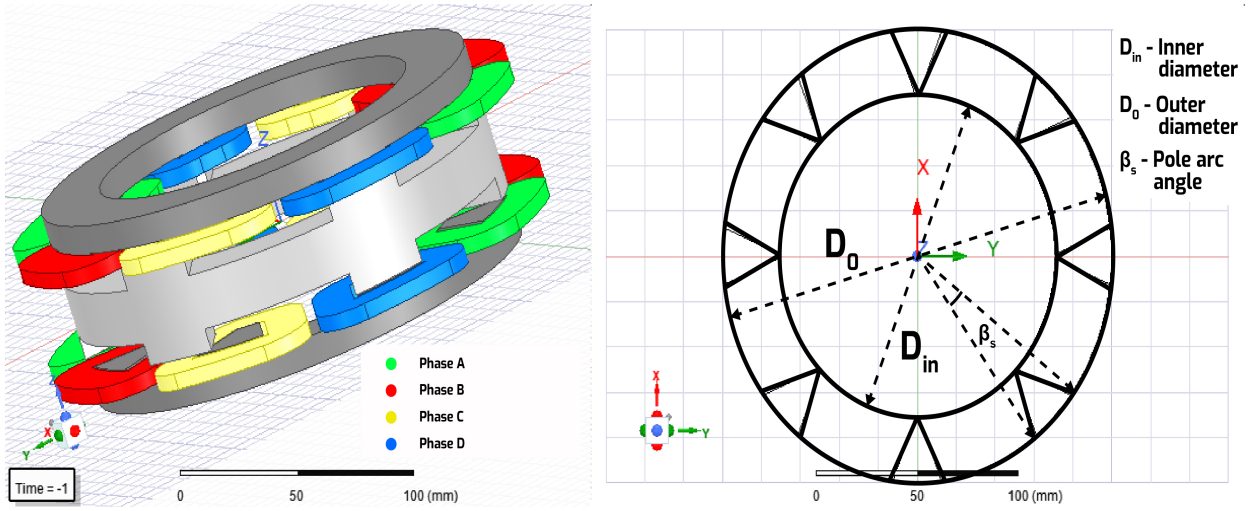

(a) (b)

Figure 1. (a) 8\6\8 pole single-tooth winding conventional DSAFSRM. (b) Rotor or stator dimensions.

The rotor comprises 6 teeth on each side of stator. These teeth are connected to the rotor core, which is the return path of the flux coming from stator. Each stator has 8 poles, with concentrated winding wound in it for excitation. The winding polarities, while in aligned position, avail the flux to flow through stator poles to gap then to rotor tooth returning from rotor core to the rotor tooth (which is in aligned position on other side), and from there it returns back to stator through air gap and completes its loop by flowing back to stator pole through stator core.

The following equation gives minimum value of β_s as given in Fig. 1(b) corresponding to minimum value of inner diameter. For a particular minimum value of arc at given inner diameter, the shape of rotor tooth will be approximately triangular as shown in Fig. 1(b).

$$D_{in} \sin\left(\frac{180}{N_s}\right) = D_o \sin\left(\frac{180}{N_s} - \frac{\beta_{smin}}{2}\right) \tag{1}$$

D_{in} = Inner stator diameter

D_o = Outer stator diameter

β_s = Arc angle of stator

β_{smin} = Minimum value of arc angle of stator pole

N_s = Number stator pole on each side

$$w = D_o \sin\left(\frac{180}{N_s} - \frac{\beta_s}{2}\right) \tag{2}$$

Here w in Equation (2) is the value of $Bs1$ and $Bs2$ in slot types 3 and 5 shown in Figs. 2(a) and 2(b).

(a) (b)

Figure 2. (a) Slot type 3 in RMxpert. (b) Slot type 5 in RMxpert.

The inter dependency of stator tooth arc angle on its inner diameter as shown in Equation (1) limits the modification in stator tooth arc angle. A 4-phase 8\6\8 pole single-tooth winding DSAFSRM has been taken as the baseline DSSRM in this paper to improve its torque pulsation behaviour. Design process is followed as given in [26]. As only half of flux flows from stator core, the height of stator is taken such that the area of stator core is half of the area of stator tooth. Similarly, the area of rotor core is taken equal to the area of rotor tooth, because the same amount of flux flows through rotor core. Table 1 lists the design parameters of this baseline DSAFSRM. The baseline DSAFSRM is preserved as DSAFSRM, and the proposed model is presented as DSAFSRM3 in this paper. The multi-level air gap without pole shoe is also analysed which is presented as DSAFSRM2. The dynamic response of the DSAFSRM has been simulated at the rated speed with the peak phase current of 38 A. The average torque (T_{avg}) and % torque ripple (% T_{ripple}) are 10.23 N m and 107.46%, respectively. This investigation shows the presence of high torque ripples in this motor and demands for further mitigation of torque ripple.

Table 1. 8\6\8 pole DSAFSRM design data.

Parameter	Value
Number of lower stator poles/rotor segments/upper stator poles	**8\6\8**
Outer and inner diameter of stator and rotor	**200 and 145 mm**
Yoke height of stator	**11.37 mm**
Yoke height of rotor	**21.91 mm**
Stator teeth length	**7 mm**
Axial length (l)	**77.66 mm**
Arc angle of stator (β_s)	**19 deg**
Length of air-gaps (l_g)	**0.5 mm**
Number of conductors/slot (N_{slot})	**45**
Rated speed	**1200 rpm**
Peak phase current	**38 A**
Stroke angle and number of strokes per revolution	**15 deg and 24**

2. TORQUE RIPPLE ANALYSIS OF CONVENTIONAL DSAFSRM

The major causes for the torque ripple generation in an SRM are: (a) edge flux; (b) local saturation of the exciter magnetic poles and the rotor pole due to the double salient pole structure; (c) the phase current and torque jump are caused by switching power converter circuit in switched reluctance motor system [24, 25]. These three aspects lead to inherent torque ripple problem in the SRM.

$$T = \frac{i^2}{2}\frac{\partial L}{\partial \theta} \tag{3}$$

Torque drop is mainly during the commutation of two phases as shown in Fig. 3. As in one phase current started decreasing, and in another phase it started increasing. In this situation, net torque decreases as the phase in which current is increasing produces less torque because of saturation during the initial overlapping of rotor and stator teeth. So to decrease the torque ripple, $\frac{\partial L}{\partial \theta}$ should increase in both the phases.

Therefore to increase $\frac{\partial L}{\partial \theta}$ when current is increasing in the phase, saturation problem that occurs during initial overlapping position needs to be mitigated as this causes low torque and torque ripple issue. In the proposed model, multilevel air gap with pole shoe is used to shape the inductance profile so as to mitigate the torque ripple. This model not only solves the saturation problem during initial overlapping but also shifts the peak static torque towards right as shown in Fig. 13, which means that the maximum torque will be produced by the phase when the phase is turned off. This torque profiling is achieved with the help of different levels of air gap form by modifying rotor geometry.

Figure 3 shows the total instantaneous torque profile, current, and inductance profile of different phases in single plot. The current profile of phases can be identified from the hysteresis band around 38 A. All the remaining curves are of the inductance of the different phases. The parametric analysis can be carried out to mitigate the ripple in the developed torque by varying the variables such as the width of pole shoe, arc angle, and turn on and turn off angles. Optimization method used for reducing torque ripple is iterative as shown in Fig. 4. Design parameters, turn on and pulse width are varied till the optimum performance parameter (lower torque ripple) are also derived.

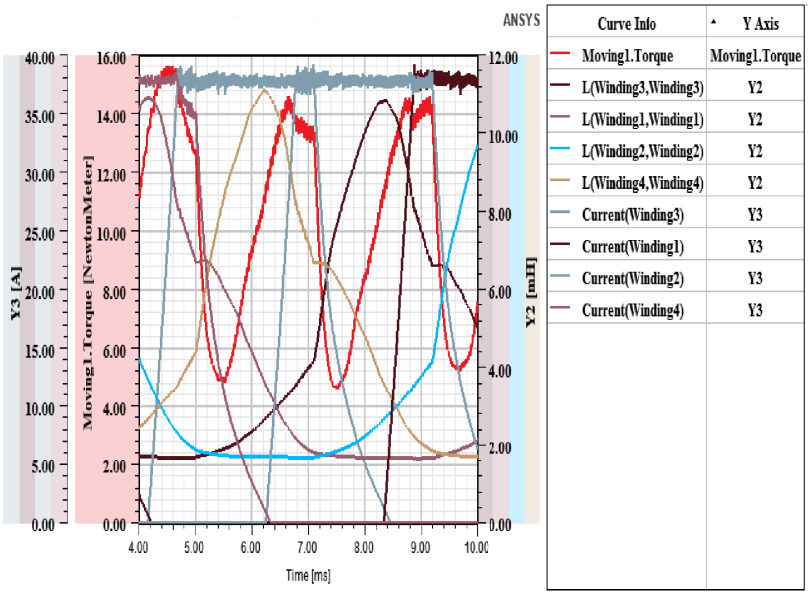

Figure 3. Total Instantaneous Torque in red colour, current and inductance profile of the phases are shown with different colour.

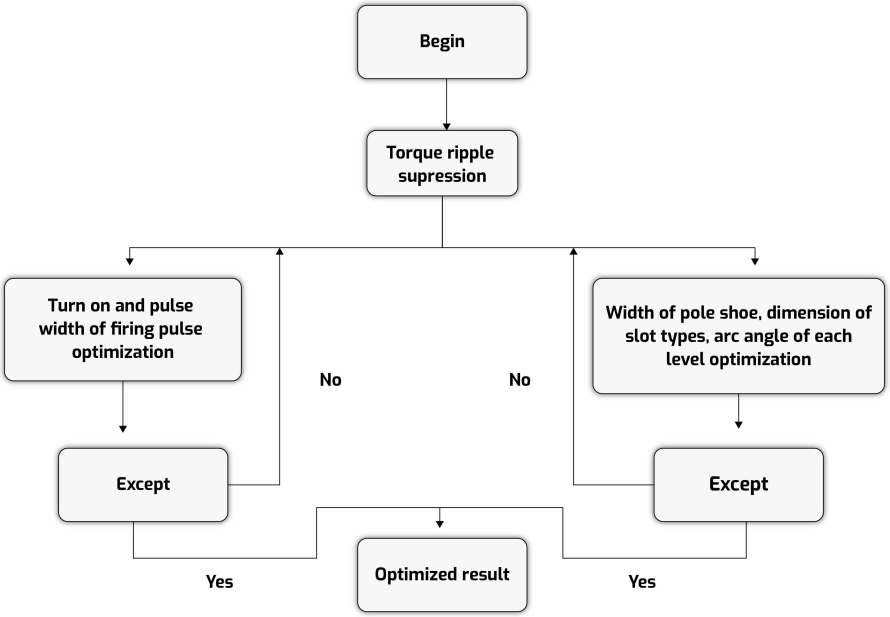

Figure 4. Flowchart of optimization method used.

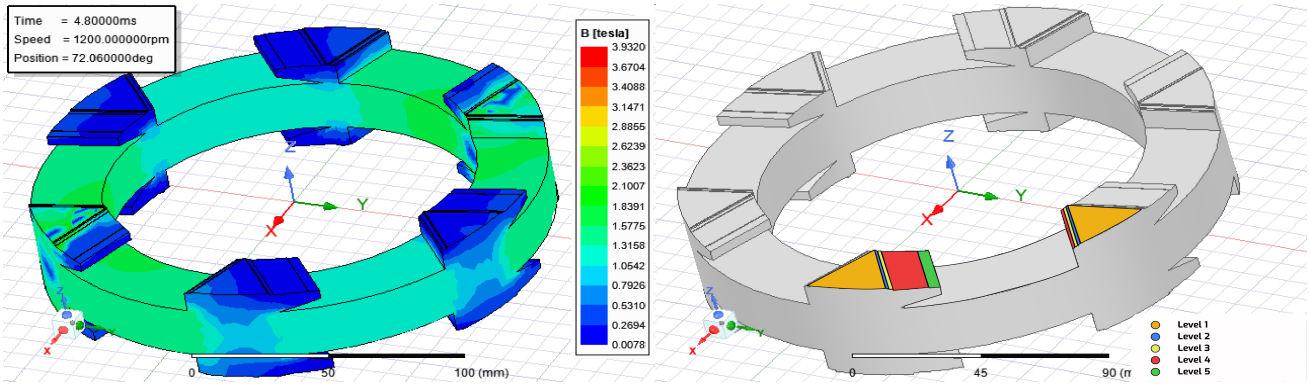

(a) (b)

Figure 5. Rotor of proposed model.

3. PROPOSED GEOMETRIC MODIFICATIONS IN DSAFSRM

Two types of modification are proposed in rotor with an aim to reduce torque ripples as shown in Fig. 5

(i) Pole shoe.

(ii) Multilevel air gap.

In this study, a multilevel air gap with a single wedge pole shoe in each rotor tooth is used. The increase in the air-gap magnetic flux can increase minimum torque and reduce the torque ripple [35]. The limitations of the power electronic converter is also a major cause of torque ripple in high speed region [27–29]. The torque developed in SRM depends on excitation current and inductance. The multi-level air gap design technique fits the appropriate air gap dimensions at each position to produce a variable inductance along the air gap, thus meeting the demanded torque [34]. A torque sharing function controls the input current of different phases to shape output torque whereas the multi-level

air gap design focuses on geometric shaping of the poles. It is well known that the air gap length has a significant impact on output performance of AFSRMs, and it is actually one of the most important optimization parameters in the machine design process. Smaller air gaps increase the inductance at the aligned position, but the unaligned inductance remains unaffected. It can be depicted that the torque profiles of machines change with the variation of air gap length.

3.1. Modification in the Rotor tooth

3.1.1. Multi-Level Air Gap

At first, the multi-level air gap technique is used to mitigate the torque ripple. For multiple level air gaps, our rotor is made of three level air gaps. Fig. 6 represents the B-H curve of the material of stator and rotor core. Table 2 describes the dimension slots for different levels of air gap. For all levels slot type 3 is used. The shaping of the rotor is done by manipulating $Bs1$, $Bs2$, and also $Hs2$. Values of other parameters in slot types 3 are taken as 0. After forming three different rotor of the dimensions as given in Table 2, unite command available in the Maxwell 3-D is used to form a single rotor of different levels of air gap at different pole arc angles. It is deduced from the static analysis that the static torque profile of DSAFSRM2 is flatter at the top than conventional motor static torque profile as shown in Fig. 8. As the current in the phase starts decreasing, the drop in torque will be slower than DSAFSRM. DSAFSRM static torque profile is peaky due to saturation, as shown in Fig. 9. When the current decreases, the torque decreases rapidly because of which large torque ripples are present in DSAFSRM. From Fig. 7 it is confirmed that in DSAFSRM2 torque ripple decreases from 107.46% to 86.78%.

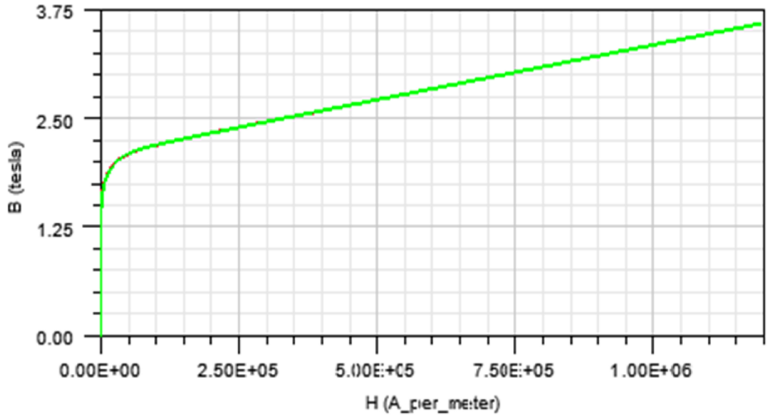

Figure 6. BH curve of steel material available in library.

Table 2. Dimensions of rotor slots of five different rotors to form three level of air gaps.

Level of air gap	Air gap	Type of slot	Pole arc angle ($Bs1 = Bs2$)	$Bs0$	$Hs0$	$Hs1$	$Hs2$
Level 1	**0.5 mm**	**Type 3**	**17.5 deg**	**72.4876 mm**	**0 mm**	**0 mm**	**10.25 mm**
Level 2	**0.65 mm**	**Type 3**	**18 deg**	**71.6735 mm**	**0 mm**	**0 mm**	**10.1 mm**
Level 3	**1.15 mm**	**Type 3**	**20 deg**	**68.4040 mm**	**0 mm**	**0 mm**	**9.6 mm**

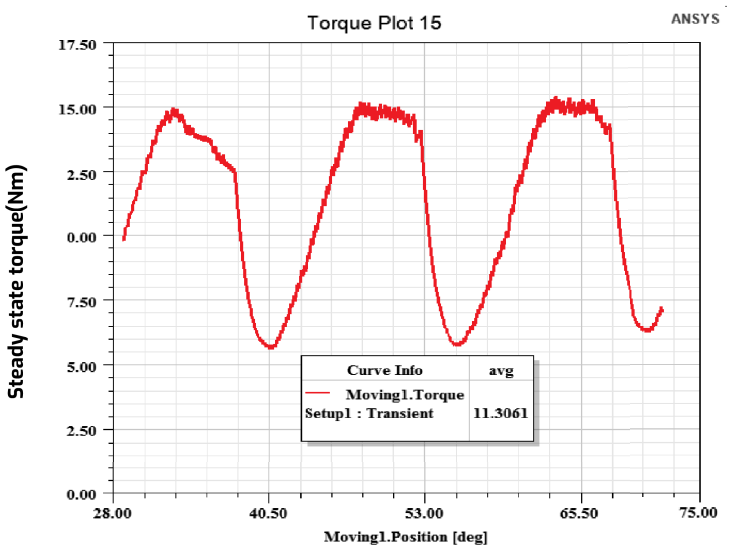

Figure 7. Steady State torque of DSAFSRM2.

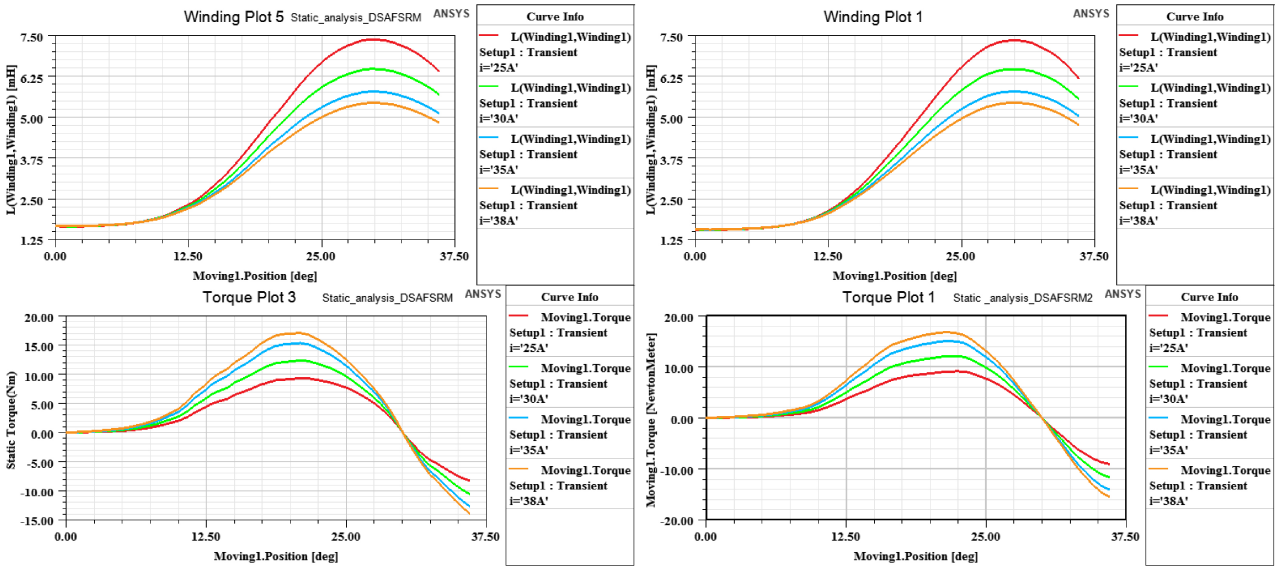

Figure 8. Top left Static inductance of DSAFSRM, top right static inductance profile of DSAFSRM2, bottom left static torque profile of DSAFSRM and bottom right is static torque profile DSAFSRM2 for different values of current.

3.1.2. Analytical Calculation of Aligned Inductance for DSAFSRM

Each phase is formed by connecting the four coils in series. As during aligned position most of the reluctance is offered by air, for our calculation purpose saturation of rotor and stator is neglected. Therefore, the inductance at aligned position can be given by Equation (4).

$$L_{al} = 4 * \frac{N_{slot}^2}{R_g} \tag{4}$$

$$R_g = \frac{l_g}{\mu_0 A_g} \tag{5}$$

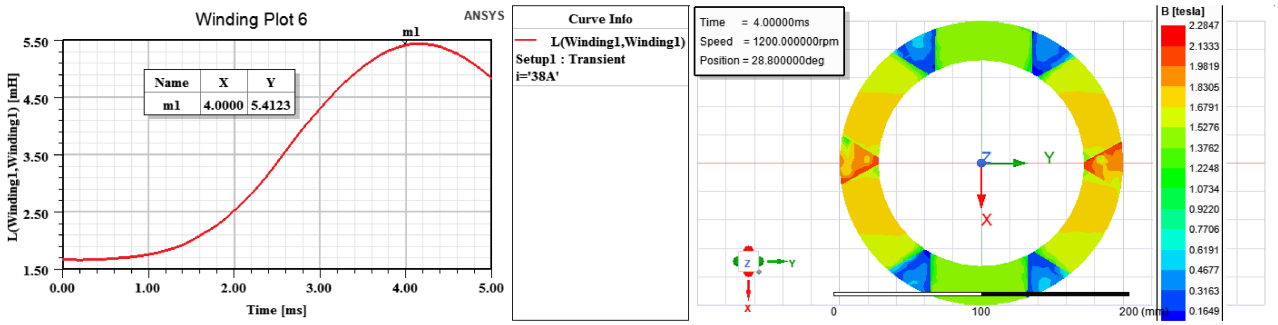

Figure 9. (a) Static inductance profile and (b) flux density distribution of DSAFSRM at aligned position for peak current 38 A.

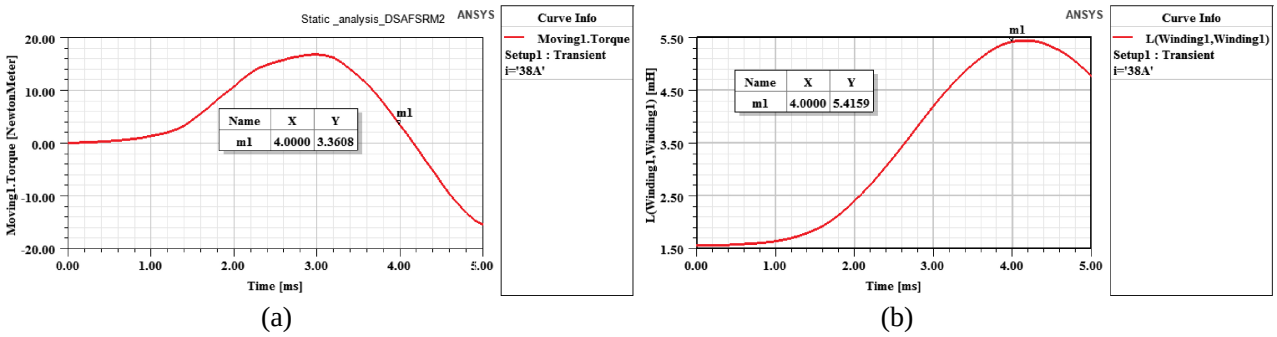

Figure 10. (a) Static torque profile and (b) static inductance profile of DSAFSRM2 for peak current.

A_g is the air gap area which is approximately equal to stator pole area. L_{al} is calculated as 12.72 mH by above equation. From FEM results L_{al} is about 11.2 mH, at average value of current in one phase, which is less than calculated value because of saturation in poles of stator and rotor as shown in Fig. 9.

3.1.3. Static Analysis

B-H curve of the material used for stator and rotor is given in Fig. 6. Therefore, the material used for rotor and stator will get saturated at 1.7 T. Flux density distribution is plotted in rotor poles of DSAFSRM and DSAFSRM2 as shown in Figs. 9 and 10. Fig. 11 depicts the flux density distribution plot of DSAFSRM3 whereas Fig. 12 represents the rotor pole shape forming of DSAFSRM3. In the flux density distribution plot at aligned position of rotor and stator, DSAFSRM rotor tooth is more saturated than DSAFSRM2 rotor tooth. The change in torque as a function of current i and position θ can be approximately given by 6. Torque profile, for constant value of current, remains nearly constant as θ changes for some region, which then decreases rapidly from point **m1** as shown in Fig. 10. This nearly constant static torque profile helps reducing torque during phase commutation, meaning when the current value is depleting in the phase as shown in Fig. 8.

$$\delta T(i,\theta) = \frac{\partial T}{\partial \theta}\delta\theta|_{i=\text{const}} + \frac{\partial T}{\partial i}\delta i|_{\theta=\text{const}} \tag{6}$$

3.1.4. Multi-Level Air Gap with Pole Shoe

For multiple level air gaps our rotor is made of five level air gaps in proposed model. The performance parameters of DSAFSRM and DSAFSRM2 are shown in Table 3. Table 4 lists the design data of DSAFSRM2 whereas Table 6 shows the design data of the proposed DSAFSRM3. For two lower level

Table 3. Performance data for 8\6\8 pole DSAFSRM and DSAFSRM2.

Parameter	DSAFSRM	DSAFSRM2
Rated speed (N)	1200 rpm	1200 rpm
Phase turn-on delay angle in degree (mech.)	0	0
Phase turn-off angle in degree (mech.)	21.14	22.729
Output torque (T_{avg})	10.23 N m	11.30 N m
Copper losses	370.15 W	409.88 W
Core losses	66.29 W	65.46 W
Output power	1285.53 W	1419.99 W
Efficiency	74.65%	74.92%

Table 4. 8\6\8 pole DSAFSRM2 design data.

Parameter	Value
Number of lower stator poles/rotor segments/upper stator poles	8\6\8
Outer and inner diameter of stator and rotor	200 and 145 mm
Yoke height of stator	11.37 mm
Yoke height of rotor	23.55 mm
Axial length (l)	79.3 mm
Arc angle of stator (β_s)	19 deg
Length of air-gap (l_g)	0.5 mm
Number of conductors/slot (N_{slot})	45
Rated speed	1200 rpm
Peak phase current	38 A
Stroke angle and number of strokes per revolution	15 deg and 24

Table 5. Dimensions of rotor slots of five different rotors to form five level air gap.

Level of air gap	Air gap	Pole arc angle ($Bs1 = Bs2$)	$Bs0$	$Hs0$	$Hs1$	$Hs2$
Level 1	0.5 mm	17.5 deg	72.4876 mm	0 mm	0 mm	10.25 mm
Level 2	0.65 mm	18 deg	71.6735 mm	0 mm	0 mm	10.1 mm
Level 3	1.15 mm	20 deg	68.4040 mm	0 mm	0 mm	9.6 mm
Level 4	1.45 mm	21 deg	54.7613 mm	1.8703 mm	0 mm	6.3 mm
Level 5	1.75 mm	21 deg	50.7613 mm	1.8703 mm	4.5879 mm	1.4120 mm

air gaps slot type 5 is used, and for other levels slot type 3 is used. After forming different rotors of dimensions as shown in Table 5, the unite command available in Maxwell 3-D is used to form a single rotor having different air gaps at different arc angles. Level 5 of rotor tooth gives the total height of 9 mm. The total height of rotor tooth considering all the level is 10.25 mm.

The arc angles of last two levels are the same, but the values of $Bs0$ and $Hs2$ are different for

Table 6. 8\6\8 pole DSAFSRM3 design data.

Parameter	Value
Number of lower stator poles/rotor tooth/upper stator poles	8/6/8
Outer and inner diameter of stator and rotor	200 and 145 mm
Yoke height of stator	11.37 mm
Yoke height of rotor	23.55 mm
Axial length (l)	81.3 mm
Arc angle of stator (β_s)	19 deg
Length of stator teeth	7 mm
Length of air-gaps (l_g)	0.5 mm
Number of conductors/slot (N_{slot})	45
Rated speed	1200 rpm
Peak phase current	38 A
Stroke angle and number of strokes per revolution	15 deg and 24

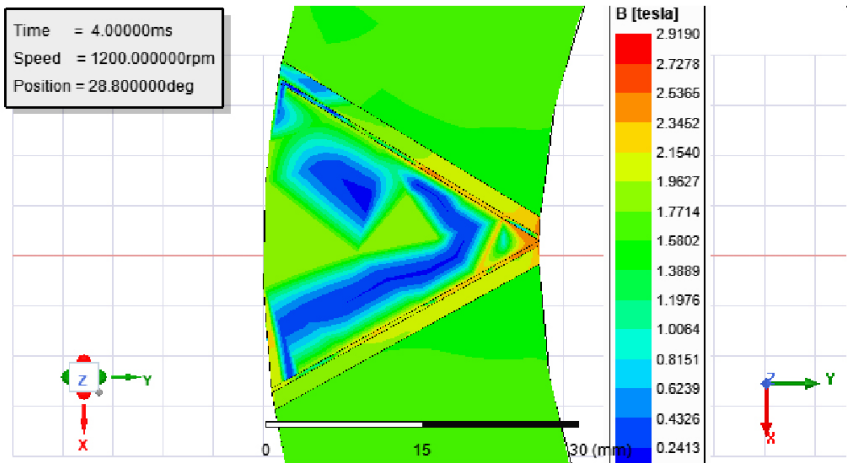

Figure 11. Flux density distribution of DSAFSRM2 at aligned position for constant current excitation 38 A.

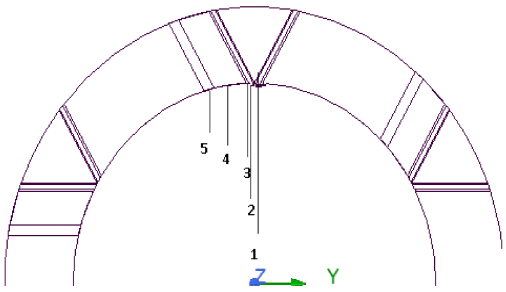

Figure 12. DSAFSRM3 rotor pole shape showing different arc angle for different levels.

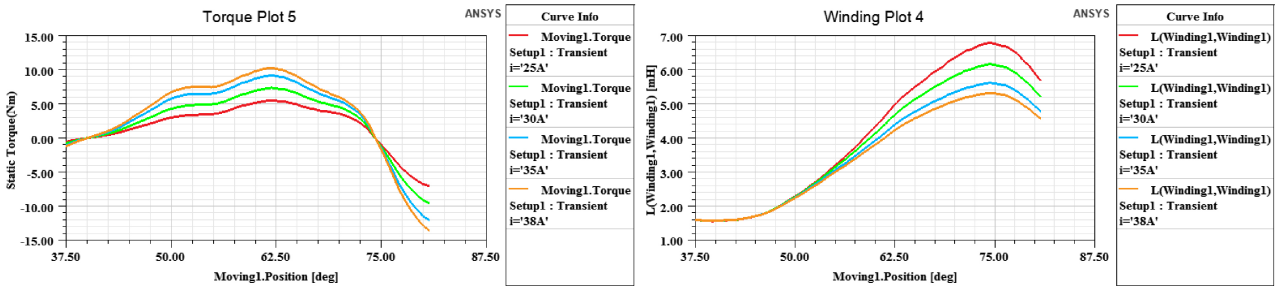

Figure 13. (a) Static torque of DSAFSRM3 for different values of excitation current and (b) static inductance profile of DSAFSRM3 for different values of excitation current.

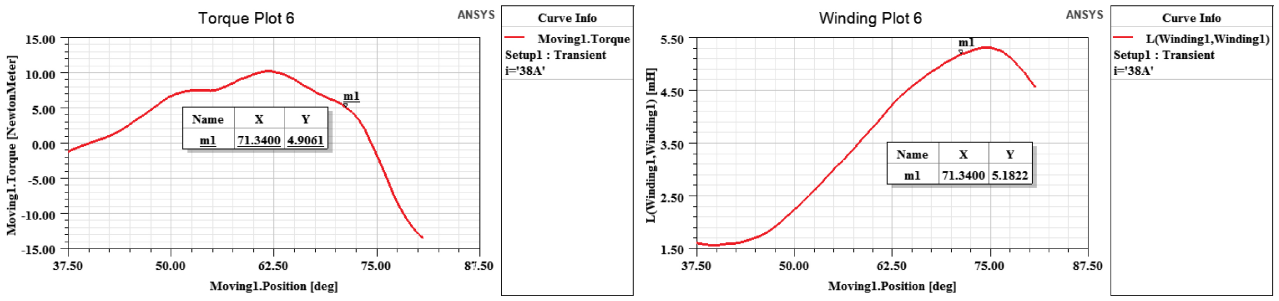

Figure 14. (a)Variation of moving torque with moving rotor position and (b) static inductance profile for DSAFSRM3 with moving rotor position.

adding one more level of air gap at the pole shoe. By giving different values of pole arc angle $Bs1$ and $Bs2$ values can be manipulated. For different levels of air gap the value of $Hs2$ is manipulated. In this way, the rotor poles for different levels of air gaps at different arc angles can be shaped. The values of other parameters in slot types 3 are taken as 0 for preparing the conventional stator and rotor poles. In proposed model, for slot type 5, the values of $Bs0$, $Hs0$, $Hs1$, and $Hs2$ are taken as the variable parameter to reduce torque ripple.

3.1.5. Static Analysis

The static analysis of the proposed model proves that the static torque profile is flatter at top than DSAFSRM2 as shown in Figs. 13 and 10. Flatter static torque profile is the objective for lesser torque ripples. The reduced torque ripple in proposed model compared to that of DSAFSRM2 is evident from Fig. 16(b). It can be seen that the peak torque producing area is shifted right in static torque curve of DSAFSRM3 as shown in Fig. 13. It remains constant for some region, then rises to peak value after it decreases slowly to point **m1** as shown in Fig. 14, and then decreases rapidly from point **m1**. Peak torque shifted rightward helps reducing the torque ripple in the commutation region when current drops in the phase. From Fig. 13 as current decreases, peak torque also decreases, but that reduction will be less than the static torque profile of DSAFSRM as shown in Fig. 8.

4. FINITE-ELEMENT MODELLING AND SIMULATION RESULTS

The design parameters of conventional DSAFSRM is shown in Table 1. The modifications in the parameters for the conventional DSAFSRM proposed are discussed in Section 3. The efficacy of the modified design is validated by 3D finite-element modelling owing to its high accuracy. The electromagnetic analysis is carried out using ANSYS\MAXWELL software. Asymmetric half bridge converter is used as a driving circuit for the analysis of both the conventional DSAFSRM and

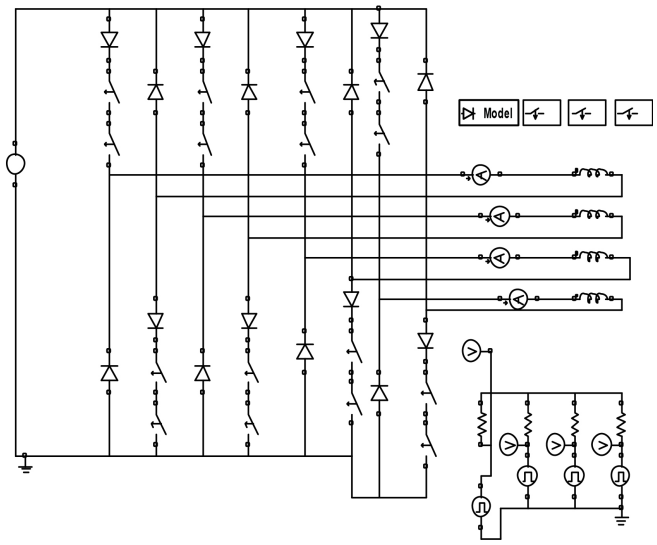

Figure 15. Maxwell circuit.

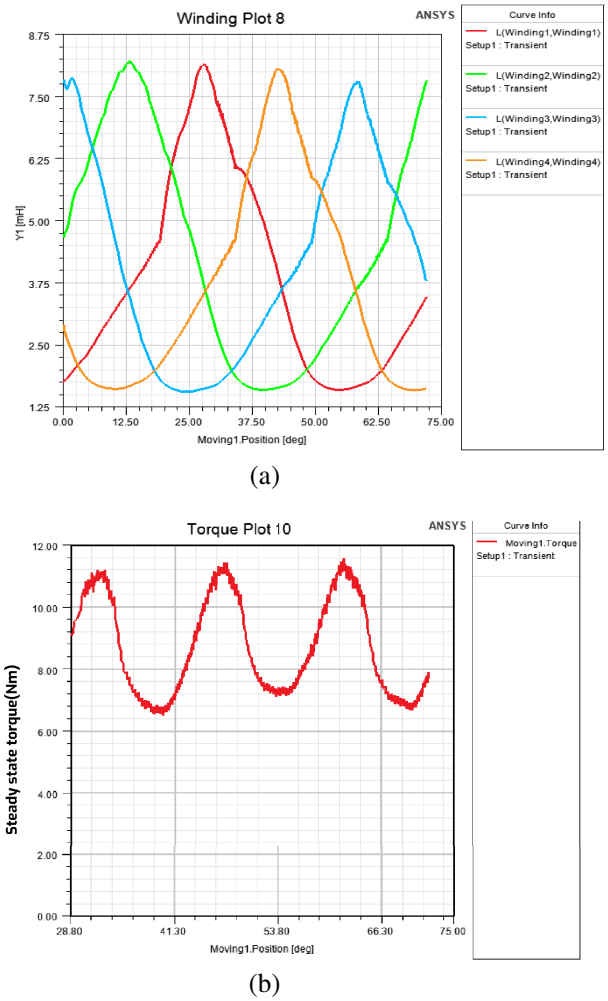

Figure 16. (a) Steady state inductance profile of DSAFSRM3. (b) Steady state torque of DSAFSRM3.

modified DSAFSRM. However, other converter topologies are also available in literature [23]. In the presented paper, phase current is limited by employing Hysteresis control with the bandwidth of 0.5 A. Equation (7) gives the details to measure the torque ripple. Four phases of motor are connected to the external circuit with voltage source of 113 V in the electrical circuit analysis. Fig. 15 gives the circuit diagram of circuit which is imported from Maxwell circuit.

$$T_{ripple} = \frac{T_{pk2pk}}{T_{avg}} \tag{7}$$

$$\eta = \frac{output\_power}{output\_power + total\_losses} \tag{8}$$

where T_{pk2pk} is the difference between maximum torque and minimum torque, and T_{avg} is the average torque. Here η in Equation (8) denotes the efficiency. Total losses comprise core losses and copper losses. Material properties are defined according to the method used for calculating the losses. To calculate core losses B-P curve method is used. The bulk conductivity of copper is taken as 58000000 Siemens/m.

It can be seen from Fig. 13 that the static torque profile of the proposed model is smoother and flat at top due to which torque ripples are less in DSAFSRM than DSAFSRM3. Fig. 9 shows the steady state response of proposed model. For high output torque and low torque ripple, the phase current overlapping technique is used in both cases. The values of T_{avg} and % T_{ripple} are 10.23 N-m and 107.46%, respectively, in the case of DSAFSRM. It reveals the presence of a high torque ripple in this motor. The values of T_{avg} and % T_{ripple} are 8.73 N-m and 51.84%, respectively, in the case of

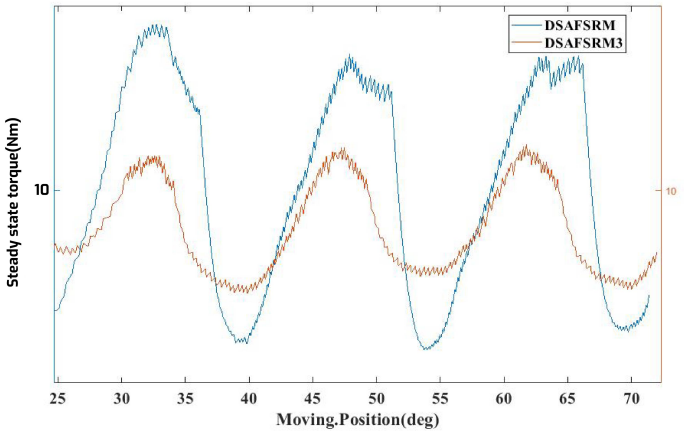

Figure 17. Comparison figure for conventional DSAFSRM and DSAFSRM3.

Table 7. Performance data for 8/6/8 pole DSAFSRM and DSAFSRM3.

Parameter	DSAFSRM	DSAFSRM3
Rated speed (N)	1200 rpm	1200 rpm
Phase turn-on delay angle in degree (mech.)	0	−3.53
Phase turn-off angle in degree (mech.)	21.14	19.17
Output torque (T_{avg})	10.23 N m	8.73 N m
Torque ripple (T_{ripple})	107.46%	51.84%
Copper losses	370.15 W	331.42 W
Core losses	66.29 W	56.47 W
Output power	1285.53 W	1097.04 W
Efficiency	74.65%	73.87%

DSAFSRM3. It discloses that the torque ripple is significantly reduced in this case, as shown in Fig. 17. Table 7 deals with the comparative data of DSAFSRM and DSAFSRM3 for rated speed.

5. CONCLUSION

This paper proposes an improved 8\6\8 pole DSAFSRM for torque ripple mitigation. In the proposed DSAFSRM, multi-level air gap technique is used to reduce the torque ripple. Geometrical modification is uniformly applied to all the rotor teeth, so as to achieve different levels of air gap to get required torque during phase commutation. Comparative analysis of the proposed DSAFSRM with that of baseline DSAFSRM is presented in the paper. It is worth noting that the proposed DSAFSRM has a significant mitigation in torque ripple. The multi-level air gap design minimizes the ripple in the developed torque while maintaining the smoother average output torque. The procedures for these design modifications are comprehensively discussed and validated by a 3D FEM model of the proposed motor which is established in ANSYS\MAXWELL software. The torque ripples in the baseline and proposed DSAFSRM are observed to be 107.46% and 51.84%, respectively. It can also be expressed that torque ripple reduction is 55.62% in the proposed DSAFSRM for the rated operating condition. It is observed that the efficiency of the proposed DSAFSRM (73.87%) is slightly less than the conventional DSAFSRM (74.65%). The proposed motor can be employed for low torque ripple applications.

ACKNOWLEDGMENT

The authors are thankful to the research grant from Science and Engineering Research Board, India under SERB POWER FELLOWSHIP Grant No. SPF/2021/000071. This work was also supported by project grant No. EEQ/2021/000057 extended by SERB, India.

REFERENCES

1. Chiba, A., K. Kiyota, N. Hoshi, M. Takemoto, and S. Ogasawara, "Development of a rare-earth-free SR motor with high torque density for hybrid vehicles," *IEEE Transactions on Energy Conversion*, Vol. 30, No. 1, 175–182, March 2015.
2. Gerada, D., A. Mebarki, N. L. Brown, C. Gerada, A. Cavagnino, and A. Boglietti, "High-speed electrical machines: Technologies, trends, and developments," *IEEE Transactions on Industrial Electronics*, Vol. 61, No. 6, 2946–2959, June 2014.
3. Ling, X., B. Li, L. Gong, Y. Huang, and C. Liu, "Simulation of switched reluctance motor drive system based on multi-physics modeling method," *IEEE Access*, Vol. 5, 26184–26189, 2017.
4. Han, G., H. Chen, and G. Guan, "Low-cost SRM drive system with reduced current sensors and position sensors," *IET Electric Power Applications*, Vol. 13, No. 7, 853–862, July 2019.
5. Sun, Q., J. Wu, C. Gan, Y. Hu, N. Jin, and J. Guo, "A new phase current reconstruction scheme for four-phase SRM drives using improved converter topology without voltage penalty," *IEEE Transactions on Industrial Electronics*, Vol. 65, No. 1, 133–144, January 2018.
6. Krishnan, R., S.-Y. Park, and K. Ha, "Theory and operation of a four-quadrant switched reluctance motor drive with a single controllable switch-the lowest cost four-quadrant brushless motor drive," *IEEE Transactions on Industry Applications*, Vol. 41, No. 4, 1047–1055, July–August 2005.
7. Gan, C., J. Wu, Q. Sun, W. Kong, H. Li, and Y. Hu, "A review on machine topologies and control techniques for low-noise switched reluctance motors in electric vehicle applications," *IEEE Access*, Vol. 6, 31430–31443, 2018.
8. Mishra, A. K. and B. Singh, "Self-governing single-stage photovoltaic water pumping system with voltage balancing control for a four-phase SRM drive," *IET Electric Power Applications*, Vol. 14, No. 1, 119–130, January 2020.
9. Borg Bartolo, J., M. Degano, J. Espina, and C. Gerada, "Design and initial testing of a high-speed 45-kW switched reluctance drive for aerospace application," *IEEE Transactions on Industrial Electronics*, Vol. 64, No. 2, 988–997, February 2017.

10. Ho, C., J. Wang, K. Hu, and C. Liaw, "Development and operation control of a switched- reluctance motor driven flywheel," *IEEE Transactions on Power Electronics*, Vol. 34, No. 1, 526–5537, January 2019.
11. Liang, J., L. Jian, G. Xu, and Z. Shao, "Analysis of electromagnetic behavior in switched reluctance motor for the application of integrated air conditioner on-board charger system," *Progress In Electromagnetics Research*, Vol. 124, 347–364, 2012.
12. Isobe, K., K. Nakamura, and O. Ichinokura, "A consideration of high speed SR motor for electric power tools," *Journal of the Magnetics Society of Japan*, Vol. 38, No. 5, 194–198, 2014.
13. Mecrow, B. C., E. A. El-Kharashi, J. W. Finch, and A. G. Jack, "Segmental rotor switched reluctance motors with single-tooth windings," *IEE Pro. — Electric Power Applications*, Vol. 150, No. 5, 591–599, September 9, 2003.
14. Hayashi, H., K. Nakamura, A. Chiba, T. Fukao, K. Tungpimolrut, and D. Dorrell, "Efficiency improvements of switched reluctance motors with high-quality iron steel and enhanced conductor slot fill," *IEEE Transactions on Energy Conversion*, Vol. 24, No. 4, 819–825, December 2009.
15. Li, Y., S. Ravi, and D. C. Aliprantis, "Tooth shape optimization of switched reluctance motors for improved torque profiles," *Power & Energy Society General Meeting*, 1–7, July 26–30, 2015.
16. Jing, L. and J. Cheng, "Research on torque ripple optimization of switched reluctance motor based on finite element method," *Progress In Electromagnetics Research M*, Vol. 74, 115–123, 2018.
17. Li, Q., A. Xu, L. Zhou, and C. Shang, "A deadbeat current control method for switched reluctance motor," *Progress In Electromagnetics Research Letters*, Vol. 91, 123–128, 2020.
18. Wang, S., Z. Hu, and X. Cui, "Research on novel direct instantaneous torque control strategy for switched reluctance motor," *IEEE Access*, Vol. 8, 66910–66916, 2020.
19. Deng, X., B. Mecrow, H. Wu, and R. Martin, "Design and development of low torque ripple variable-speed drive system with six-phase switched reluctance motors," *IEEE Transactions on Energy Conversion*, Vol. 33, No. 1, 420–429, March 2018.
20. Cao, X., J. Zhou, C. Liu, and Z. Deng, "Advanced control method for a single-winding bearingless switched reluctance motor to reduce torque ripple and radial displacement," *IEEE Transactions on Energy Conversion*, Vol. 32, No. 4, 1533–1543, December 2017.
21. Chen, C., H. Guo, and G. Zhang, "SOSM direct torque and direct suspension force control for double stator bearingless switched reluctance motor," *Progress In Electromagnetics Research C*, Vol. 96, 179–192, 2019.
22. Gecer, B. and N. F. O. Serteller, "Understanding switched reluctance motor analysis using ANSYS/Maxwell," *2020 IEEE 29th International Symposium on Industrial Electronics (ISIE)*, 446–449, Delft, Netherlands, 2020.
23. Miller, T. J. E., *Switched Reluctance Motors and Their Control*, CRC Press, London, U.K., 1993.
24. Lawrenson, P. J., J. M. Stephenson, and P. T. Blenkinsop, "Variable-speed switched reluctance motors," *Electric Power Applications IEE Proceedings B*, Vol. 127, No. 4, 253–265, July 1980.
25. Li, Z., L. Zheng, and W. Yang, "Research on torque ripple and structure optimization of switched reluctance motor," *Electric Machines and Control.*, Vol. 22, No. 6, 11–21, July 2018.
26. Krishnan, R., M. Abouzeid, and X. Mang, "A design procedure for axial field switched reluctance motors," *IEEE 1990 Industry Applications Society Annual Meeting*, 241–246, 1990.
27. Ye, J., B. Bilgin, and A. Emadi, "An offline torque sharing function for torque ripple reduction of switched reluctance motor drives," *IEEE Transactions on Energy Conversion*, Vol. 30, No. 2, 726–735, June 2015.
28. Lin, J., N. Schofield, and A. Emadi, "External-rotor 6–10 switched reluctance motor for an electric bicycle," *Proc. IECON*, 348–356, 2013.
29. Li, H., E. Fairall, B. Bilgin, and A. Emadi, "Performance evaluation of a high-speed high-power switched reluctance motor drive," *Proc. APEC*, 1337–1342, 2015.
30. Gupta, T. D., K. Chaudhary, R. M. Elavarasan, R. K. Saket, I. Khan, and E. Hossain, "Design modification in single-tooth winding double-stator switched reluctance motor for torque ripple mitigation," *IEEE Access*, Vol. 9, 19078–19096, 2021, doi: 10.1109/ACCESS.2021.3052828.

31. Das Gupta, T. and K. Chaudhary, "Research on torque ripple minimization of double-stator switched reluctance motor using finite element method," *Advances in Electrical and Computer Engineering*, Vol. 21, No. 4, 135, 2021.
32. Das Gupta, T. and K. Chaudhary, "Finite element method based design and analysis of a low torque ripple double-stator switched reluctance motor," *Progress In Electromagnetics Research C*, Vol. 111, 191–206, 2021.
33. Li, Q., A. Xu, L. Zhou, and C. Shang, "A deadbeat current control method for switched reluctance motor," *Progress In Electromagnetics Research Letters*, Vol. 91, 123–128, 2020.
34. Lin, J., T. Lambert, Y. Yang, B. Bilgin, R. Lankin, and A. Emadi, "A novel axial flux switched reluctance motor with multi-level air gap geometry," *2016 IEEE Electrical Power and Energy Conference (EPEC)*, 1–8, 2016, doi: 10.1109/EPEC.2016.7771732.
35. Huang, C., J. Duan, W. Liu, and Y. Wu, "Optimizing turn-on angle and external rotor pole shape to suppress torque ripple of a novel switched reluctance motor," *Progress In Electromagnetics Research M*, Vol. 107, 243–257, 2022.